**Atmospheric
Chemistry
and Physics**

Technical Note: Recipe for monitoring of total ozone with a precision of around 1 DU applying mid-infrared solar absorption spectra

M. Schneider and F. Hase

IMK-ASF, Forschungszentrum Karlsruhe, Karlsruhe, Germany

Abstract. Mid-infrared solar absorption spectra recorded by a state-of-the-art ground-based FTIR system have the potential to provide precise total O_3 amounts. The currently best-performing retrieval approaches use a combination of small and broad spectral O_3 windows between 780 and 1015 cm^{-1}. We show that for these approaches the uncertainties of the temperature profile are by far the major error sources. We demonstrate that a joint optimal estimation of temperature and O_3 profiles widely eliminates this error. The improvements are documented by an extensive theoretical error estimation. Our results suggest that mid-infrared FTIR measurements can provide total O_3 amounts with a precision of around 1 DU, placing this method among the most precise ground-based O_3 monitoring techniques. We recapitulate the requirements on the instrumental hardware and on the retrieval that are needed to achieve this high precision.

1 Introduction

The demand for very high precision measurements of atmospheric constituents is recently increasing. Many aspects of stratospheric ozone destruction (and recovery) or the evolution of atmospheric greenhouse gases are well understood. However, a closer look reveals important uncertainties. Concerning ozone recovery, it is not clear how climate change will affect the future evolution of the upper tropospheric and stratospheric ozone amounts. Consequently, it cannot be foreseen how, when, and to what extent ozone recovery will take place (Weatherhead and Andersen, 2006). A continuous O_3 monitoring at very high precision is important for further scientific progress. Such activities are indispensable to document potential differences between the real and a modeled atmosphere in due time.

Correspondence to: M. Schneider
(matthias.schneider@imk.fzk.de)

Ground-based measurements yielding highly-resolved infrared solar absorption spectra allow ongoing detection of the composition of the atmosphere in a cost-effective manner. They are essential for validating satellite measurements and, thus, they are a vital component of the global atmospheric monitoring system. Ongoing improvements in instrumental hardware, spectroscopic parameterisation, and retrieval strategies steadily increase the FTIR data quality. In this work we estimate the potential of high quality middle infrared spectra for a precise monitoring of total O_3 amounts. The estimations base on the spectra quality routinely achieved with a Bruker IFS 125HR at the Izaña Observatory, Canary Island of Tenerife, Spain. In the following sections we describe the current state-of-the-art O_3 profile retrieval (De Mazière et al., 2004) and estimate its errors. The error estimation motivates to set up a new retrieval strategy, which includes the optimal estimation of temperature profiles. We predict that the new approach should allow for the retrieval of FTIR O_3 column amounts with a precision of around 1 DU. In Sect. 4 we summarize in detail the requirements on the instrumental hardware and the kind of retrieval strategy necessary in order to achieve this high precision.

2 Optimal estimation of O_3 profiles

2.1 Retrieval strategy

We apply an optimal estimation (OE) method (Rodgers, 2000) to invert the profiles from the measured FTIR spectra by minimising the cost function:

$$\sigma^{-2}(\boldsymbol{y}-\mathbf{K}\boldsymbol{x})^T(\boldsymbol{y}-\mathbf{K}\boldsymbol{x}) + (\boldsymbol{x}-\boldsymbol{x_a})^T\mathbf{S_a}^{-1}(\boldsymbol{x}-\boldsymbol{x_a}) \qquad (1)$$

The first term considers the information present in the spectra assuming a diagonal noise covariance ($\mathbf{K}$, $\boldsymbol{x}$, $\boldsymbol{y}$, and σ represent Jacobian, the atmospheric state, the spectrum, and the measurement noise, respectively). The second term accounts
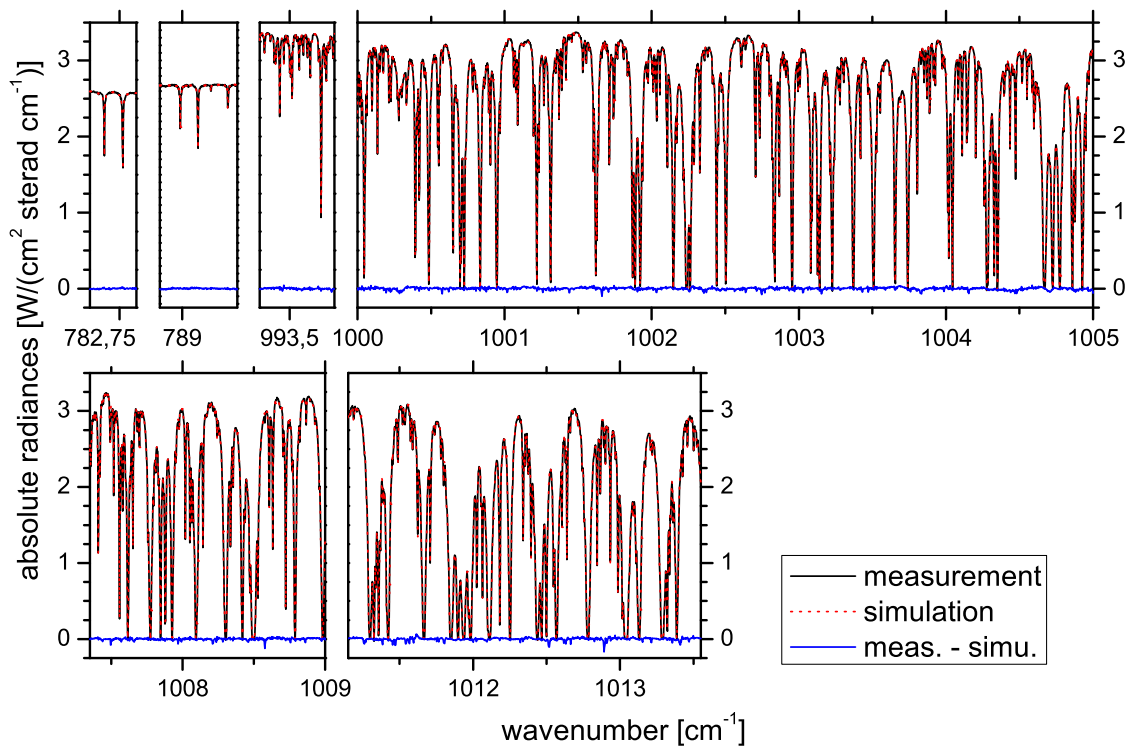
Fig. 1. Spectral windows applied. Plotted is the situation for a real measurement taken on 22nd of January 2005 (solar elevation angle 32.2°); black line: measured spectrum; red line: simulated spectrum; blue line: difference between simulation and measurement.

for the a-priori knowledge: S_a is the a-priori covariance matrix and x_a represents the a-priori state. We apply the inversion code PROFFIT (Hase et al., 2004) which uses the Karlsruhe Optimised and Precise Radiative Transfer Algorithm (KOPRA, Höpfner et al., 1998; Kuntz et al., 1998; Stiller et al., 1998) as forward model.

We use spectral microwindows with $^{48}O_3$ and asymmetric and symmetric $^{50}O_3$ and $^{49}O_3$ absorption signatures in the mid-infrared (between 780–1015 cm^{-1}; see Fig. 1). In the 782.75 and 789.0 cm^{-1} windows only the main isotopologue ($^{48}O_3$) has absorption signatures. There are also minor interferences from CO_2, H_2O, and solar lines. These two microwindows are the same that were used in Schneider et al. (2005). The strongest line in the 993.5 cm^{-1} window is a symmetric $^{50}O_3$ signature (at 993.8 cm^{-1}). Other signatures are from $^{48}O_3$, asymmetric $^{50}O_3$, symmetric and asymmetric $^{49}O_3$, H_2O, CO_2, and solar lines. Broadband microwindows are very useful to improve the sensitivity of the observing system for the lower troposphere (Barret et al., 2002). We apply three broadband microwindows between 1000.0 and 1013.6 cm^{-1}. In these microwindows all $^{48}O_3$, $^{50}O_3$, and $^{49}O_3$ isotopologues have absorption signatures. The main interfering species are H_2O and CO_2.

We make an OE of $^{48}O_3$, asymmetric, and symmetric $^{50}O_3$ and of the isotopologue ratio profiles of $^{48}O_3/^{50}O_3$. The latter is an option recently introduced in PROFFIT (Schneider

et al., 2006), which provides for an improved constraint of the resulting profiles. As a-priori of O_3 (mean profile and covariances) we use a climatology of Izaña's ECC-sondes from 1996 to 2006. However, in this and the following section we show that the choice of the a-priori is a minor error source and consequently our conclusions are not limited to Izaña. As a-priori for the typical ozone isotopologue ratio profiles and their covariances we use data reported by Johnson et al. (2000). The spectral signatures of the minor isotopologues of $^{49}O_3$ are only considered by scaling a climatological profile. The H_2O interferences are considered by scaling an actual H_2O profile as retrieved in a previous step from specific H_2O microwindows of the same measurement. This H_2O retrieval is described in Schneider et al. (2006). The minor signatures of CO_2 and C_2H_4 are considered by scaling corresponding climatological profiles.

The applied temperature data are a combination of the data from the local ptu-sondes (up to 30 km) and data supplied by the automailer system of the Goddard Space Flight Center. The spectroscopic line parameters of H_2O and of O_3 are taken from the HITRAN 2004 database (Rothman et al., 2005). For all other species we apply HITRAN 2000 parameters (Rothman et al., 2003). To minimise errors due to uncertainties of the instrumental line shape we monitor and eventually correct line shape distortions regularly every two months. These measurements consist in independent

detections of cell absorption signatures as described in Hase et al. (1999). The σ of Eq. (1) is taken from the residuals of the fit itself, performing an automatic adjustment of the constraints according to the noise level found in each measurement.

2.2 Error estimation

Our error analysis bases on the analytic method suggested by Rodgers (2000), where the difference between the retrieved and the real state $(\hat{x}-x)$ — the error — is linearised about a mean profile x_a, the estimated model parameters $\hat{p}$, and the measurement noise ϵ:

$$
\begin{aligned}
\hat{x}-x = \quad & \\
& (\hat{\mathbf{A}}-\mathbf{I})(x-x_a) \\
& + \hat{\mathbf{G}}\hat{\mathbf{K}}_{\mathbf{p}}(p-\hat{p}) \\
& + \hat{\mathbf{G}}\epsilon
\end{aligned} \tag{2}
$$

Here $\mathbf{I}$ is the identity matrix, $\hat{\mathbf{A}}$ the averaging kernel matrix, $\hat{\mathbf{G}}$ the gain matrix, and $\hat{\mathbf{K}}_{\mathbf{p}}$ a sensitivity matrix to model parameters. Equation (2) identifies the three classes of errors. These are: (a) errors due to the inherent finite vertical resolution of the observing system (smoothing error), (b) errors due to uncertainties in the input parameters applied in the inversion procedure, and (c) errors due to measurement noise (with standard deviation ϵ).

Generally one assumes linearity of the forward model within the range of the variability of the atmospheric state. Then the errors are calculated according to Eq. (2) applying single mean matrices for $\hat{\mathbf{A}}$, $\hat{\mathbf{G}}$, and $\hat{\mathbf{K}}_{\mathbf{p}}$. However, for the saturated (or nearly saturated) spectral O_3 lines as shown in Fig. 1 the Jacobians depend on the actual atmospheric state. Therefore, we use an ensemble of 500 real states which obeys the a-priori statistics and calculate for each individual members of this ensemble the matrices $\hat{\mathbf{A}}$, $\hat{\mathbf{G}}$, and $\hat{\mathbf{K}}_{\mathbf{p}}$: we make for each of the 500 real states an individual error estimation according to Eq. (2).

An error estimation should distinguish systematic and random errors. Generally one defines the global mean and standard deviation of a large ensemble of errors as the systematic and the random error component. However, this global treatment disregards that the errors may depend on the actual atmospheric state or the observing geometry. For example, an error may depend on the actual atmospheric O_3 distribution: an optimal estimation approach constrains towards a climatological a-priori amount. This constraint favours positive errors in O_3 amounts below the a-priori amount and negative errors in O_3 amounts above the a-priori amount. In this section we examine the dependence of the errors on the total O_3 amounts. In addition an error may depend on the strength of the absorption signal. This strength is determined by the O_3 slant column amount, i.e. by a combination of the actual O_3 distribution and the observing geometry. In Sect. 3 we show how the errors depend on the O_3 slant column amounts.

Figure 2 depicts the errors versus the O_3 amounts. We separate the random and systematic errors by means of a least squares fit. The regression curve of a least squares fit gives the systematic error, i.e. it documents how the observing system as a mean reflects the real atmospheric situation. It seems sufficient to apply linear least squares fits. One systematic error is the difference of the slope of the regression line from zero. It shows how the observing system systematically under- or overestimates the real variabilities. We call this error "sensitivity error". It is significant for uncertainties in the temperature profiles and the line parameters (for more details see Sect. 2.2.2). Another systematic error component can be seen as an offset of the regression line. This 'bias error' is due to systematic error sources or incorrect a-priori assumptions. The values we give as bias error refer to the offset of the regression line at the a-priori value (climatological value). It is in particular large for errors due to intensity offsets, uncertainties in the temperature profile, and uncertainties in the line intensities. The scattering around the regression line gives the random error. The correlation coefficient of the linear least squares fit is linked to the scattering around the regression line (e.g. Wilks, 1995):

$$
\sigma_{\epsilon\mathrm{reg}} = \sigma_\epsilon \sqrt{1-\rho^2} \tag{3}
$$

Here $\sigma_{\epsilon\mathrm{reg}}$ is the scattering around the regression line, i.e. the random error component, σ_ϵ is the scattering of the ensemble values, and ρ the correlation coefficient. For more details about this method of error calculations please consult Schneider et al. (2006).

2.2.1 Smoothing error

According to Eq. (2) the smoothing error is given by $(\hat{\mathbf{A}}-\mathbf{I})(x-x_a)$. The upper left panel of Fig. 2 shows the correlation between O_3 amount and the smoothing error. The smoothing error has no systematic bias error component (no offset at the a-priori value). This is trivial, since we use as a-priori the same statistics that was applied for the simulation of the ensemble profiles. However, it is not trivial that there is nearly no systematic sensitivity error (slope of regression line of 0.998). This nearly perfect sensitivity demonstrates that the choice of the a-priori has a negligible impact on the retrieved O_3 amounts. The random error component is 0.36 DU. The estimated systematic and random smoothing errors are listed together with the other errors in Table 2.

2.2.2 Input parameter errors

In this subsection errors due to uncertainties in solar angle, instrumental line shape (ILS: modulation efficiency and phase error Hase et al., 1999), baseline of the spectrum (intensity offset), temperature profile, and spectroscopic parameters (line intensity and pressure broadening coefficient) are estimated. The assumed parameter uncertainties ($p-\hat{p}$) are listed in Table 1.
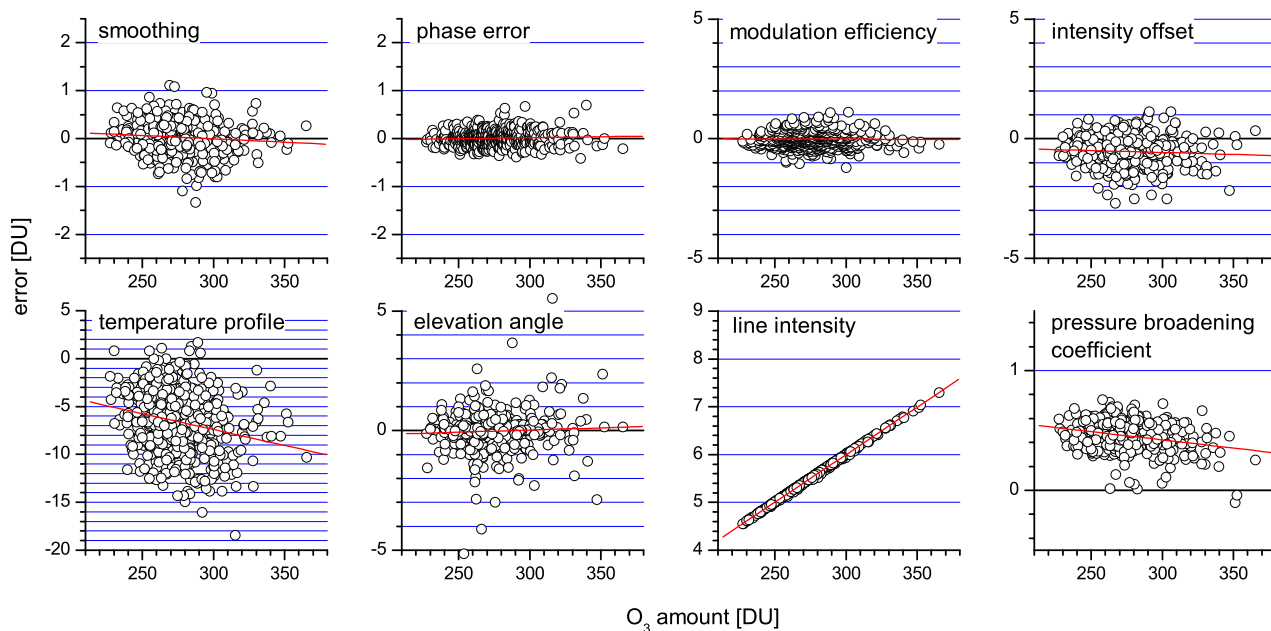
Fig. 2. Errors of retrieved total O3 amounts versus total O_3 amounts. Circles represent the 500 individual members of the applied ensemble. The red lines are the linear regression lines. The blue griding is the same in every panel and helpful to identify the relative importance of the error.

Table 1. Assumed uncertainties.

error source		random	systematic
phase error		0.01 rad	–
modulation eff.		1 %	–
intensity offset		0.1 %	+0.1 %
T profile	at surface	1.7 K	−3.5 K
	rest of troposphere	0.7 K	–
	at 30 km	1 K	up to +4 K
	above 50 km	6 K	up to −12 K
solar angle		0.1°	–
line intensity		–	−2 %
pres. broad. coef.		–	−2 %

$^{\alpha}$detailed description see text

We estimate the ILS stability from regularly performed low pressure N_2O cell measurements (Hase et al., 1999), to 0.01 rad for the phase error and 1% for the modulation efficiency. An intensity offset may be caused by detector non-linearities. Here we use a photo-voltaic MCT detector instead of the usually applied photo-conductive detectors. It has the advantage of reduced non-linearities and thus an improved zero baseline determination (less spectral intensity offset). We estimate the spectral intensity offset in our spectra by analysing very intense O_3 signatures between 1024.25 and 1025 cm^{-1}. Those signatures are saturated even for O_3 slant columns as low as 250 DU. We found a mean offset

of 0.1 % and a standard deviation of 0.1 % in the core of the saturated lines. Two sources are considered as random uncertainty in the temperature profile: first, the measurement uncertainty of the sonde, which is assumed to be 0.5 K throughout the whole troposphere and to have no interlevel correlations. Second, the temporal differences between the FTIR and the sonde's temperature measurements, which are estimated to be 1.5 K at the surface and 0.5 K in the rest of the troposphere, with a correlation length of 5 km. Furthermore, we assume systematic errors in the temperature profile (for more details please see Sect. 3).

The parameter errors are calculated according to Eq. (2) by $\hat{\mathbf{G}}\hat{\mathbf{K}}_{\mathbf{p}}(\boldsymbol{p}-\hat{\boldsymbol{p}})$. Subsequently we estimate their systematic and random components by correlation to the O_3 amounts. The correlations are shown in Fig. 2. The systematic and random errors are estimated as for the smoothing error: from the slope and bias of the regression line and the correlation coefficient (see Eq. 3). The assumed uncertainties of Table 1 lead to large random and systematic errors due to uncertainties in the temperature profile (random: 3.5 DU; sensitivity error: −3.3 %; bias: −7.0 DU). We also made these simulation assuming no systematic error in the temperature profile, i.e. assuming no error for the temperature dependence of the pressure broadening coefficient. In this case the random error remains unchanged at 3.5 DU, but the systematic components reduce significantly: to −1.6 % for the sensitivity error and to −0.2 DU for the bias. Although reduced, there is still a systematic sensitivity error even in the absence of a systematic temperature error source.

Error sources of minor importance are the intensity offset, solar elevation angle, and modulation efficiency (0.4, 0.3 and 0.3 DU, respectively). All other random errors are negligible, i.e. are situated below 0.2 DU. Significant systematic errors are produced by errors in the line intensity parameter (error of 2 % column amount error for 2 % parameter error) and due to an intensity offset (error of -0.2 % for assumed systematic offset of 0.1 %). A systematic error in the pressure broadening coefficient causes only very small systematic errors in the column amounts. All errors are collected in Table 2.

2.2.3 Measurement noise error

This error is due to statistical fluctuation in the measured signal, caused by e.g. photon noise or thermal noise in the detector or noise produced by the signal amplification. It causes white noise in the residuals. With the Bruker IFS 125HR and the applied photo-voltaic MCT detector we reach a signal to noise ratio of typically 1000 around $1000\,cm^{-1}$. We found this value by analysing measured spectra in regions with no absorption issues. Its impact on total column amounts is negligible. Our simulations lead to errors below 0.1 DU (see Table 2).

3 Simultaneous optimal estimation of O₃ and temperature profiles

Table 2 reveals that uncertainties in the assumed temperature profile are mainly responsible for the overall errors in the retrieved columns amounts. Both the shape and the area of an absorption line depend on the temperature. Thus, errors in the temperature profile lead to erroneous simulations of the line shapes and areas and consequently to errors in the retrieved trace gas profiles.

The applied inversion code PROFFIT allows a joint optimal estimation of temperature profile together with VMR profiles. From the viewpoint of the forward model, the retrieval of temperature brings in several complications: the absorption cross sections cannot be precomputed before the iterative retrieval process is performed, instead recalculation in each iteration step is required. Derivatives of temperature have to be provided at each model level. The construction of the temperature derivatives within the forward model KOPRA used here, is described in Stiller et al. (2000). Finally, as hydrostatic equilibrium is assumed, it has to be taken into account that a change of the temperature profile implicates a modified pressure stratification. Therefore, in each iteration step an atmosphere in hydrostatic balance is reconstructed and the pressure at each altitude fixed model level is changed according to the current temperature profile. From the viewpoint of the retrieval, the joint fit of temperature requires extensions to the state vectors, the Jacobian and the a-priori covariances. An a-priori temperature profile and associated a-priori covariance have to be provided by the user

Table 2. Estimated random (in DU) and systematic errors (sensitivity in % and bias in DU) of the total column amounts.

error source	random	systematic (sensitivity/bias)
smoothing	0.4 DU	-0.2 %/–
phase error	0.1 DU	–/–
modulation eff.	0.3 DU	–/–
intensity offset	0.4 DU	-0.2 %/-0.6 DU
temperature	3.5 DU	-3.3 %/-7.0 DU
solar angle	0.3 DU	–/–
line intensity	–	$+2.0$ %/$+5.8$ DU
pres. broad. coef.	0.1 DU	-0.1 %/$+0.5$ DU
measurement noise	0.1 DU	–/–
total	3.5 DU	

as additional input. The a-priori temperature profiles used here are a combination of the daily ptu-sonde and the Goddard NCEP temperatures as described in Sect. 2. The a-priori temperature covariance is constructed in accordance with the assumed random error budget of the temperature profile (see Table 1). The reasons for the random temperature errors have been discussed in Sect. 2. We also found systematic differences between our optimally estimated temperature profiles and the ptu-sonde/NCEP temperature profiles, which we interpret as systematic temperature errors. There are several reasons for these systematic differences: (a) the ptu-sonde is released at sea level. It already measures the temperature of the free troposphere when reaching the altitude of FTIR mountain site. In the free troposphere the temperature is generally lower than at the FTIR site. (b) At higher altitudes the sonde may give to large temperatures due to radiative heating (c) The Goddard NCEP temperatures may have systematic errors. (d) The parameterisation of the temperature dependence of the O₃ line width may be erroneous. Such a systematic error in the spectroscopic data produces systematic differences between actual and retrieved temperature profile.

We analyse how a joint optimal estimation of the temperature profiles reduces the impact of temperature uncertainties on the retrieved O₃ column amounts. We calculate for all 500 members of the ensemble the matrices $\hat{\mathbf{A}}$, $\hat{\mathbf{G}}$, and $\hat{\mathbf{K}}_{\mathbf{p}}$ for the new retrieval setup and perform the same error simulation as in Sect. 2. We found that an OE estimation of the temperature applying the O₃ windows of Fig. 1 already reduces the temperature error. However, an additional application of CO₂ windows should allow for further improvements. Spectral signatures of CO₂ are often used in remote sensing to determine temperature profiles. Atmospheric CO₂ is very stable. It has little temporal variability and its mixing ratios are nearly constant over large altitude regions. Changes in the CO₂ absorption pattern can thus be mainly attributed to changes in the temperature profile. Furthermore, CO₂ is
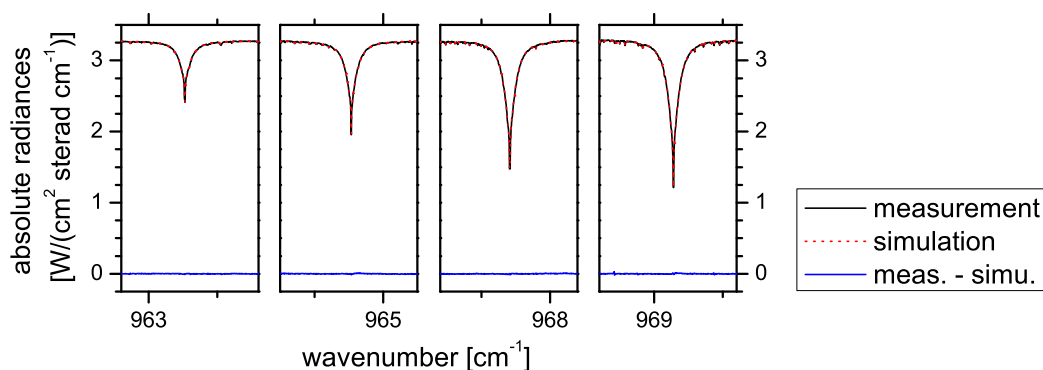
Fig. 3. Applied CO_2 windows. The spectra correspond to the same measurement as the spectra shown in Fig. 1. Scale and meaning of lines and colours is the same as in Fig. 1

Table 3. Estimated random (in DU) and systematic errors (in %) of O_3 total column amounts for simultaneous optimal estimation of O_3 and temperature profiles.

error source	random	systematic (sensitivity/bias)
smoothing	0.5 DU	–/–
phase error	0.3 DU	–/–
modulation eff.	0.7 DU	+0.1 %/–
intensity offset	0.6 DU	+0.3 %/−0.9 DU
temperature	0.1 DU	−0.2 %/−0.4 DU
solar angle	0.3 DU	–/–
line intensity	–	+2.0 %/+5.7 DU
pres. broad. coef.	0.1 DU	−0.1 %/+0.3 DU
measurement noise	0.1 DU	–/–
total	1.2 DU	

an infrared active gas and its concentrations are relatively high which assures distinct absorption signatures. We apply four spectral windows between 960 and 970 cm^{-1} containing isolated CO_2 lines of different intensities (see Fig. 3) together with the windows as described in Sect. 2 and shown in Fig. 1. The only significantly interfering absorptions in the CO_2 windows are due to O_3 and can be seen as the tiny dips in the 969 cm^{-1} window. To adjust the measured and simulated CO_2 signatures we only allow a scaling of a climatological CO_2 profile. The remaining observed residuals contain the information about the actual temperature profile.

For this retrieval setup the errors due to temperature uncertainties are widely eliminated. The random error is reduced from 3.5 DU to 0.1 DU. The systematic sensitivity error is reduced from −3.3 % to −0.2 % and the systematic bias from −7.0 DU to −0.4 DU. The smoothing error, the intensity offset, and errors due to uncertainties in the ILS and the solar elevation angle remain as leading error sources. Following the assumptions listed in Table 1 we estimate a total random error of around 1.2 DU. This is a significant improvement

over the current state-of-the-art retrieval method for which we estimate a total random error of 3.5 DU. All errors are listed in Table 3.

In Sect. 2 is has been shown how the errors typically depend on the total O_3 amounts. In this section we examine the dependence on the O_3 absorption signature. The O_3 absorption signature is determined by the O_3 slant column amount. Figure 4 shows the dependence of the errors for a simultaneous OE of O_3 and temperature. It is in particular strong for the solar elevation error. For high slant column amounts, i.e. low elevation angle, a small uncertainty of 0.1° produces errors of larger than 2 DU, whereas for low slant column amounts (or large elevation angles) these errors are below 0.2 DU. Vice versa errors due to an incorrect pressure broadening coefficient or due to uncertainties in the phase error are larger at low slant column amounts than at large slant column amounts.

Current FTIR systems are very stable experiments. Small, undetected ILS distortions or solar tracker misalignments may maintain constant over several months and are consequently systematic error sources. In Fig. 5 we characterise the errors produced by systematic uncertainties in the phase error, the modulation efficiency, the intensity offset, and the solar angle. For the modulation efficiency and the phase error we assume a systematic uncertainty of −1 % and +0.01 rad, respectively. For the intensity offset and the temperature profile we use the systematic uncertainties as listed in Table 1. This analysis completes our error characterisation. It shows that the errors produced by uncertainties in the phase error are slightly larger for low slant column amounts than for large slant column amounts: at 400 DU the errors are 0.4 DU and above 1000 DU the errors are close to 0.2 DU. A similar dependence can be observed for errors due to uncertainties in the modulation efficiency. By contrast the errors due to an intensity offset or a misalignment of the solar tracker are larger at large slant column amounts than at low slant column amounts.
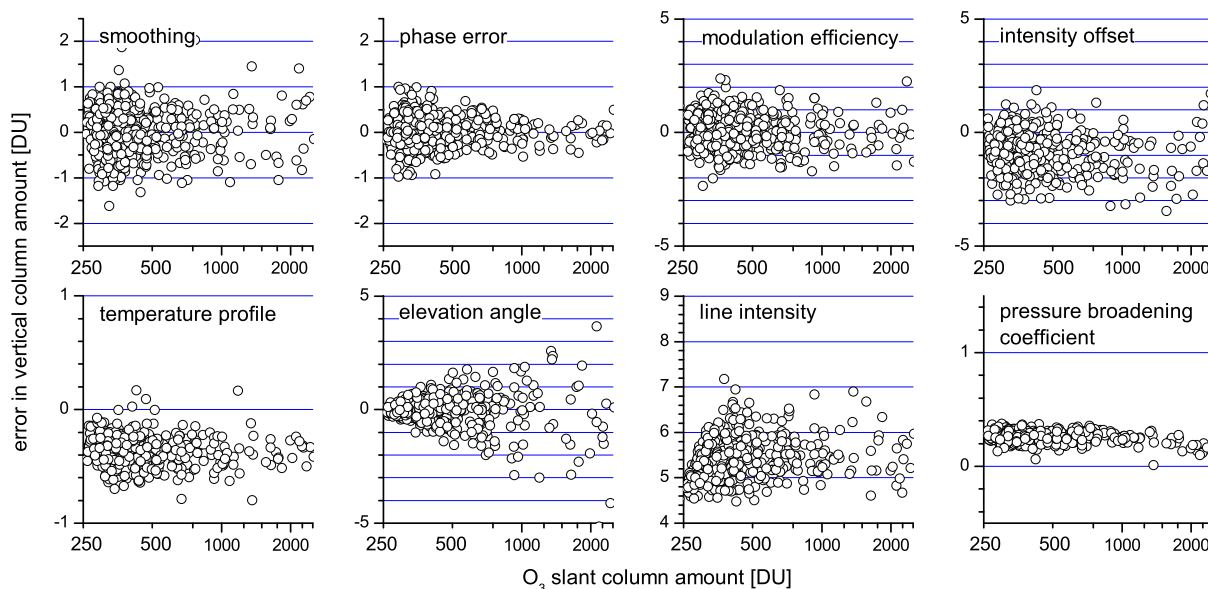
Fig. 4. Same as Fig. 2 but for new retrieval approach (i.e. simultaneous optimal estimation of O_3 and temperature profiles) and versus O_3 slant column amounts (error assumptions according to Table 1).
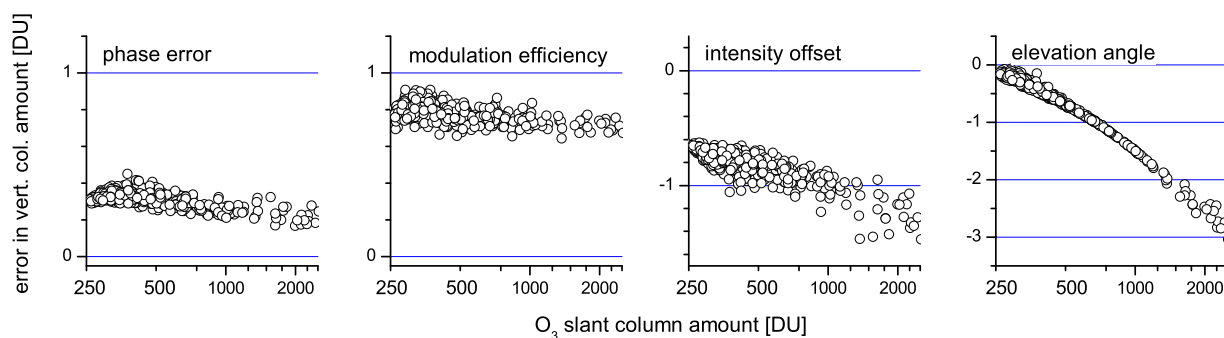

Fig. 5. Same as Fig. 4, but for only systematic error sources.

4   Summary and conclusions

Applying a state-of-the-art instrumentation and retrieval strategy provides for an estimated precision of total O_3 of around 1 DU, which converts the FTIR technique to one of the most precise techniques for a continuous monitoring of total O_3. From Table 3 we conclude that important remaining error sources are intensity offsets, small uncertainties of the ILS or of the solar elevation angle, and the smoothing error. It is, furthermore, important to state that we estimate a near ideal column sensitivity. Therefore, the applied a-priori has negligible influence on the retrieved O_3 amounts. All information about the actual O_3 content is taken from the measurement and in consequence our error estimation is of general validity and not limited to the Izaña site. The recipe is summarized as follows and contains retrieval and instrumental aspects:

(1) To eliminate the temperature error and to keep the smoothing error small it is required to apply the retrieval strategy described in the previous sections, i.e. it is mandatory to apply broad spectral windows, to perform a joint OE of $^{48}O_3$, $^{48}O_3/^{50}O_3$, and of the temperature profiles. to optimise the temperature retrieval one should introduce the spectral CO_2 windows as shown in Fig. 3. The joint OE of the temperature profile provides for the decisive improvement of the precision. Currently PROFFIT (Hase et al., 2004) is the only retrieval code for the analysis of ground-based spectra that allows to perform an OE of temperature and isotopologue profiles.

(2) One should apply a photo-voltaic instead of a photo-conductive detector. Photo-voltaic detectors have a quite linear characteristics whereas photo-conductive detectors show a certain level of non-linearity, which may offset the zero baseline of the measured spectra.

(3) One should use an instrument with a stable ILS like the Bruker IFS 120/125HR. Currently the Bruker IFS 120/125 HR spectrometers are among the best-performing FTIR spectrometers commercially available. It is difficult to achieve the required stability with portable instruments like a Bruker IFS 120M.

(4) The pointing of the solar tracker and the effective measurement time should be known with high accuracy. For a solar elevation angle of 45° an uncertainty of 0.1° in the pointing or of 30 s in the effective measurement time causes an error of 0.3 DU. For an elevation angle of 20° or 10° this error increases to 1.3 DU and 2.2 DU, respectively. At Izaña we apply a high quality home-built solar tracker. Its mirror positions are determined from astronomical calculations and additionally controlled by the signals of a quadrant detector (Huster, 1998).

(5) The intensity fluctuations during scanning should be documented. For example, clouds passing through the line of sight during scanning may cause intensity offsets in the spectra. A correction of these baseline artefacts is only possible if in addition to the AC interferogram signal the DC interferogram signal is recorded. At Izaña such a correction was not necessary due to the nearly continuous perfect clear sky conditions, however at sites with less favorable sky conditions it is indispensable.

Finally, it should be commented that a further reduction of the noise level would yield no further improvement: as shown in Table 3 the measurement noise is a negligible error source.

Edited by: A. Hofzumahaus

References

Barret, B., De Mazière, M., and Demoulin, P.: Retrieval and characterization of ozone profiles from solar infrared spectra at the Jungfraujoch, J. Geophys. Res, 107, 4788–4803, 2002.

De Mazière, M., Barret, B., Vigouroux., C., Blumenstock, T., Hase, F., Kramer, I., Camy-Peyret, C., Chelin, P., Gardiner, T., Coleman, M., Woods, P., Ellingsen, K., Gauss, M., Isaksen, I., Mahieu, E., Demoulin, P., Duchatelet, P., Mellqvist, J., Strandberg, A., Velazco, V., Schulz, A., Notholt, J., Sussmann, R., Stremme, W., and Rockmann, A.: Ground-based FTIR measurements of O_3 and climate related gases in the free troposphere and lower stratosphere, presented at the Quadrenial Ozone Symposium, 529, Kos, Greece, 2004.

Hase, F., Blumenstock, T., and Paton-Walsh, C.: Analysis of the instrumental line shape of high-resolution Fourier transform IR spectrometers with gas cell measurements and new retrieval software, Appl. Opt., 38, 3417–3422, 1999.

Hase, F., Hannigan, J. W., Coffey, M. T., Goldman, A., Höpfner, M., Jones, N. B., Rinsland, C. P., and Wood, S. W.: Intercomparison of retrieval codes used for the analysis of high-resolution, ground-based FTIR measurements, J. Quant. Spectrosc. Ra., 87, 25–52, 2004.

Höpfner, M., Stiller, G. P., Kuntz, M., Clarmann, T. v., Echle, G., Funke, B., Glatthor, N., Hase, F., Kemnitzer, H., and Zorn, S.: The Karlsruhe optimized and precise radiative transfer algorithm, Part II: Interface to retrieval applications, SPIE Proceedings 1998, 3501, 186–195, 1998.

Huster, S. M.: Bau eines automatischen Sonnenverfolgers für bodengebundene IR-Absorptionmessungen, Diplomarbeit im Fach Physik, Institut für Meteorologie und Klimaforschung, Universität Karlsruhe und Forschungszentrum Karlsruhe, 1998.

Johnson, D. G., Jucks, K. W., Traub, W. A., and Chance, K. V.: Isotopic composition of stratospheric ozone, J. Geophys. Res., 105, 9025–9031, 2000.

Kuntz, M., Höpfner, M., Stiller, G. P., Clarmann, T. v., Echle, G., Funke, B., Glatthor, N., Hase, F., Kemnitzer, H., and Zorn, S.: The Karlsruhe optimized and precise radiative transfer algorithm, Part III: ADDLIN and TRANSF algorithms for modeling spectral transmittance and radiance, SPIE Proceedings 1998, 3501, 247–256, 1998.

Rodgers, C. D.: Inverse Methods for Atmospheric Sounding: Theory and Praxis, World Scientific Publishing Co., Singapore, ISBN 981-02-2740-X, 2000.

Rothman, L. S., Barbe, A., Benner, D. C., Brown, L. R., Camy-Peyret, C., Carleer, M. R., Chance, K. V., Clerbaux, C., Dana, V., Devi, V. M., Fayt, A., Fischer, J., Flaud, J.-M., Gamache, R. R., Goldman, A., Jacquemart, D., Jucks, K. W., Lafferty, W. J., Mandin, J.-Y., Massie, S. T., Newnham, D. A., Perrin, A., Rinsland, C. P., Schroeder, J., Smith, K. M., Smith, M. A. H., Tang, K., Toth, R. A., Vander Auwera, J., Varanasi, P., and Yoshino, K.: The HITRAN Molecular Spectroscopic Database: Edition of 2000 Including Updates through 2001, J. Quant. Spectrosc. Ra., 82, 5–44, 2003.

Rothman, L. S., Jacquemart, D., Barbe, A., Benner, D. C., Birk, M., Brown, L. R., Carleer, M. R., Chackerian Jr., C., Chance, K. V., Coudert, L. H., Dana, V., Devi, J., Flaud, J.-M., Gamache, R. R., Goldman, A., Hartmann, J.-M., Jucks, K. W., Maki, A. G., Mandin, J.-Y., Massie, S. T., Orphal, J., Perrin, A., Rinsland, C. P., Smith, M. A. H., Tennyson, J., Tolchenov, R. N., Toth, R. A., Vander Auwera, J., Varanasi, P., and Wagner, G.: The HITRAN 2004 molecular spectroscopic database, J. Quant. Spectrosc. Ra., 96, 139–204, 2005.

Schneider M., Blumenstock, T., Hase, F., Höpfner, M., Cuevas, E., Redondas, A., and Sancho, J. M.: Ozone profiles and total column amounts derived at Izaña, Tenerife Island, from FTIR solar absorption spectra, and its validation by an intercomparison to ECC-sonde and Brewer spectrometer measurements, J. Quant. Spectrosc. Ra., 91, 245–274, 2005.

Schneider, M., Hase, F., and Blumenstock, T.: Ground-based remote sensing of HDO/H2O ratio profiles: introduction and validation of an innovative retrieval approach, Atmos. Chem. Phys., 6, 4705–4722, 2006,
http://www.atmos-chem-phys.net/6/4705/2006/.

Stiller, G. P., Höpfner, M., Kuntz, M., Clarmann, T. v., Echle, G.,

Fischer, H., Funke, B., Glatthor, N., Hase, F., Kemnitzer, H., and Zorn, S.: The Karlsruhe optimized and precise radiative transfer algorithm, Part I: Requirements, justification and model error estimation, SPIE Proceedings 1998, 3501, 257–268, 1998.

Stiller, G. P., Clarmann, T. v., A. Dudhia, G. Echle, B. Funke, N. Glatthor, F. Hase, M. Hpfner, S. Kellmann, H. Kemnitzer, M. Kuntz, A. Linden, M. Linder, G. P. Stiller, and S. Zorn: The Karlsruhe Optimized and Precise Radiative transfer Algorithm (KOPRA), Forschungszentrum Karlsruhe, Wissenschaftliche Berichte, Bericht Nr. 6487, 2000.

Weatherhead, E. C and Andersen, S. B.: The search for signs of recovery of the ozone layer, Nature, 441, 39–45, 2006.

Wilks, D. S.: Statistical methods in the atmospheric science, Academic Press, ISBN 0-12-751965-3, 1995.